Influence of Structural and Topological Constraints on the Crystallization and Melting Behavior of Polymers. 2. Poly(arylene ether ether ketone)

Hervé Marand,* Azar Alizadeh, Robin Farmer, Ravi Desai, and Vesselin Velikov†

Departments of Chemistry and Materials Science and Engineering, Virginia Polytechnic Institute and State University, Blacksburg, Virginia 24061-0212

Received August 11, 1999; Revised Manuscript Received February 4, 2000

ABSTRACT: The secondary crystallization and its influence on the glass transition are studied as a function of crystallization temperature and time by differential scanning calorimetry for PEEK. The multiple melting behavior resulting from isothermal annealing from the glass or crystallization from the melt is discussed in the context of models considering either a melting−recrystallization−remelting process or a bimodal population of primary and secondary crystals. The heating rate dependence of the multiple melting behavior indicates that reorganization of primary crystals occurs during heating for samples annealed from the glassy state but is insignificant for those crystallized from the melt. For either mode of crystallization, the high- and low-temperature endothermic regions are associated with the melting of primary and secondary crystals, respectively. Investigations of the low endotherm transition temperature and heat of fusion as a function of crystallization time and temperature lead to the following conclusions: the melting temperature of secondary crystals increases linearly with the logarithm of secondary crystallization time at a rate, $B(T)$, increasing linearly with decreasing temperature; the Avrami exponent, which characterizes the initial stage of secondary crystallization, is constant below ca. 310 °C ($n = {}^1/_2$) but increases gradually with temperature above 310 °C; the late stage of secondary crystallization is characterized by a linear increase in crystallinity with logarithm of time. Studies of the evolution of the glass transition after secondary crystallization indicate that the calorimetric T_g increases linearly with the logarithm of time at a rate, $b(T)$, increasing with decreasing temperature. Finally, a qualitative model of polymer crystallization of semiflexible polymer chains is proposed. This model considers the effect of structural constraints (chain stiffness) on the nature of the amorphous phase after primary crystallization and the effect of topological constraints (pinning of amorphous chains) on the secondary crystallization behavior.

Introduction

This paper is the second in a series dealing with the effect of topological constraints on the secondary crystallization behavior of polymers. In the preceding paper, we reported investigations of the morphology, crystallization, and melting behavior of random ethylene/1-octene (EO) copolymers as a function of 1-octene content.[1] In this system, the topological constraints are structural in origin and associated with the presence of hexyl branches along the polyethylene backbone. Since these branches are rejected from the polyethylene crystal lattice during quiescent crystallization, they partition the chain in crystallizable sequences of different lengths. As only the longest sequences can participate in the chain-folded lamellar growth process during primary crystallization, secondary crystallization during subsequent cooling involves predominantly the shorter crystallizable sequences of chains already pinned at the surfaces of primary crystals. These studies also demonstrated the existence of different crystallization mechanisms above and below a crossover temperature T^*, which marks the onset of primary crystallization during cooling. Below T^* the degree of crystallinity is independent of cooling rate and changes reversibly in subsequent cooling and heating cycles. In contrast, above T^* the degree of crystallinity is cooling rate dependent and exhibits hysteresis between successive cooling and heating cycles.

Isothermal secondary crystallization at any temperature T_S below T^* leads during subsequent heating to the development of an endotherm ("low endotherm") located 5−20 K above T_S but below the main endothermic transition associated with the melting of primary crystals formed during the quench to T_S. The peak temperature of this low endotherm increases linearly with the logarithm of secondary crystallization time and extrapolates to T_S at very short times. Studies of the temporal evolution of the enthalpy of fusion associated with this low endotherm indicate that the secondary crystallization process is characterized by an Avrami exponent around ${}^1/_2$, a value lower than that associated with primary crystallization above T^*. Studies of the heating rate dependence of the multiple melting phenomenon indicate that this behavior is not associated with a mechanism of melting−recrystallization−remelting. Instead, it can be explained by the melting of separate populations of crystals grown by different mechanisms as a result of changing topological constraints during solidification. Similar results and conclusions were obtained with other random ethylene/α-olefin copolymers,[2] bisphenol A polycarbonate (PC),[3] and ethylene/styrene interpolymers.[4] Morphological investigations were found to provide support for the calorimetric results and allowed us to conclude that the dual crystallization process is associated above T^* with the nucleation and growth of primary lamellar crystals from the free (i.e., unconstrained) melt and below T^* with

* To whom correspondence should be addressed. E-mail hmarand@vt.edu.

† Present address: Department of Chemistry, Arizona State University, Tempe, AZ.

10.1021/ma9913562 CCC: $19.00
Published on Web 04/04/2000

the formation of secondary fringed micellar crystals or chain cluster aggregates in a constrained environment.

The results of two-step crystallization studies below T^* led us to suggest that the upward shift of this endotherm with crystallization time is not associated with an increase in crystal perfection, lateral dimensions, or thickness but may be a consequence of the decrease in molar conformational entropy of the remaining amorphous fraction as a result of secondary crystallization.

In light of these results, we are now reporting similar studies for poly(arylene ether ether ketone) or PEEK, a polymer whose multiple endothermic behavior has received a great deal of attention in the literature[5−27] and which appears to be representative of the class of semiflexible polymers including, among others, poly(ethylene terephthalate), poly(butylene terephthalate), poly(phenylene sulfide), aliphatic polyamides, and isotactic poly(styrene).[28]

The present paper addresses the multiple melting phenomenon and the effect of secondary crystallization on the glass transition (α relaxation). The results section is organized in four parts. First, to clarify the possibility of reorganization during heating, we report studies of the melting behavior of both melt and cold crystallized PEEK as a function of heating rate. Second, we discuss the effect of crystallization time and temperature on the evolution of the low and high endotherms recorded after isothermal crystallization from the melt or from the glass. In the third section, we report two-step crystallization studies to probe the origin of secondary crystals and the nature of the time dependence of their melting behavior. In the final section, we address the effect of crystallization time and temperature on the glass transition of PEEK. In the discussion section, we examine our results in the context of a qualitative model of polymer secondary crystallization, similar to that presented for EO copolymers.[1]

Experimental Section

PEEK [IUPAC name poly(oxy-1,4-phenylene-oxy-1,4-phenylene-carbonyl-1,4-phenylene)], produced by ICI (grade 450 G, M_w = 38 300 g/mol), was obtained in the form of pellets and 0.8 mm thick amorphous plaques (Atlantic Plastic, Roanoke, VA).

Differential scanning calorimetry experiments were carried out in Perkin-Elmer DSC models 2C and 7 operated under dry nitrogen flow using a sample mass of ca. 10 mg. Crystallization temperatures were calibrated by extrapolating the melting temperature of standards (tin, lead, and indium) to zero heating rate. Melting temperatures were determined as the endotherm peak temperatures recorded at a heating rate of 10 °C/min, unless otherwise noted. Since the thermal conductivity of organic materials is much lower than that of metals, use of a pure metal standard does not lead to a rigorous calibration of the temperature scale and more importantly does not allow a proper correction of the shape of a melting endotherm for heat transfer effects. We therefore carried out the temperature calibration using an indium standard sandwiched between two amorphous PEEK films and subsequently used Gray's method[29,30] for a better accounting of the effect of heating rate on the endothermic peak shape. The heat capacity calibration was carried out using a sapphire standard after empty pan subtraction. In all cases, DSC traces are presented after subtraction of a baseline, which approximates the heat capacity of the semicrystalline sample over the temperature range considered. In the melting region, the sample heat capacity baseline was approximated by a linear function of temperature. As a result of this baseline subtraction, reported apparent heat capacities (dQ/dT) vanish above and below the melting transition. Glass transition temperatures were determined at the inflection point of heat capacity traces recorded at 10 °C/min. Isothermal crystallization experiments at a variety of temperatures were carried out in the DSC after a quench from the melt at 390 °C. Residence time in the melt prior to quenching was kept constant at 5 min. Since crystallization experiments were carried out under widely different conditions and using different strategies, we first need to define the nomenclature used in this paper. When a PEEK sample is crystallized isothermally after quenching from the melt, it is denoted MC-T_x, where the prefix MC stands from melt crystallization and T_x defines the chosen crystallization temperature. In other instances, PEEK was crystallized from the melt at temperature T_{x1} for long enough time to ensure spherulitic impingement, subsequently heated to a temperature above the low endotherm (hereafter, denoted PM for partial melting), and immediately quenched to a temperature T_{x2}, where further crystallization was allowed for different times. Such samples are denoted MC-T_{x1}-PM-SC-T_{x2} to indicate primary crystallization at T_{x1} and secondary crystallization at T_{x2} after heating above the low endotherm resulting from crystallization at T_{x1}. Some experiments were carried out by heating an initially amorphous sample at a rate of 20 °C/min from 100 °C to a temperature T_a, at which it was annealed for different times. These samples are denoted GA-T_a. Finally, GA-T_a-PM-SC-T_x denotes samples crystallized from the glass by heating to T_a. These samples were then annealed at that temperature for a given time, heated above their low endotherm transition temperature, and immediately quenched to T_x, where secondary crystallization was allowed to proceed for different times.

Results

1. Heating Rate Dependence of the Multiple Melting Behavior. In Figure 1a, corrected heating traces for a PEEK sample (MC-300) crystallized from the melt at 300 °C for 1000 min are displayed for heating rates ranging from 5 to 40 °C/min. Similar experiments were conducted with samples crystallized from the melt at 300 °C for 1000 min, partially melted by heating at 10 °C/min to 334 °C, and subsequently quenched to room temperature (Figure 1b). In Figure 2a,b, we show the evolution of the low and high endotherm peak temperatures as a function of heating rate for both series of samples. An increase in heating rate leads to an upward shift of the low endotherm but does not affect the melting temperature associated with the high endotherm, except possibly at the lowest heating rate. Within the experimental uncertainty, the total enthalpy of fusion of a given sample is independent of heating rate, and the high endotherm peak melting temperature is independent of whether the sample was partially melted or not.

We now examine the heating rate dependence of the melting behavior for a sample annealed from the glass at 300 °C for 1000 min and subsequently quenched below T_g (GA-300). The heating traces corrected with Gray's method are shown in Figure 3. The heating rate dependence of the peak location for both the low and the high endotherms are also plotted in Figure 2, a and b, respectively. While the heating rate dependence of the low endotherm position is identical within experimental error for melt and cold crystallized samples, that of the high endotherm is significantly different for these two series of samples. We also note the presence of an intermediate endotherm whose associated latent heat increases with heating rate at the expense of the highest endotherm (Figure 3).

2. Characteristics of the Low Endotherm: Low Endotherm Location. In this section, we discuss the

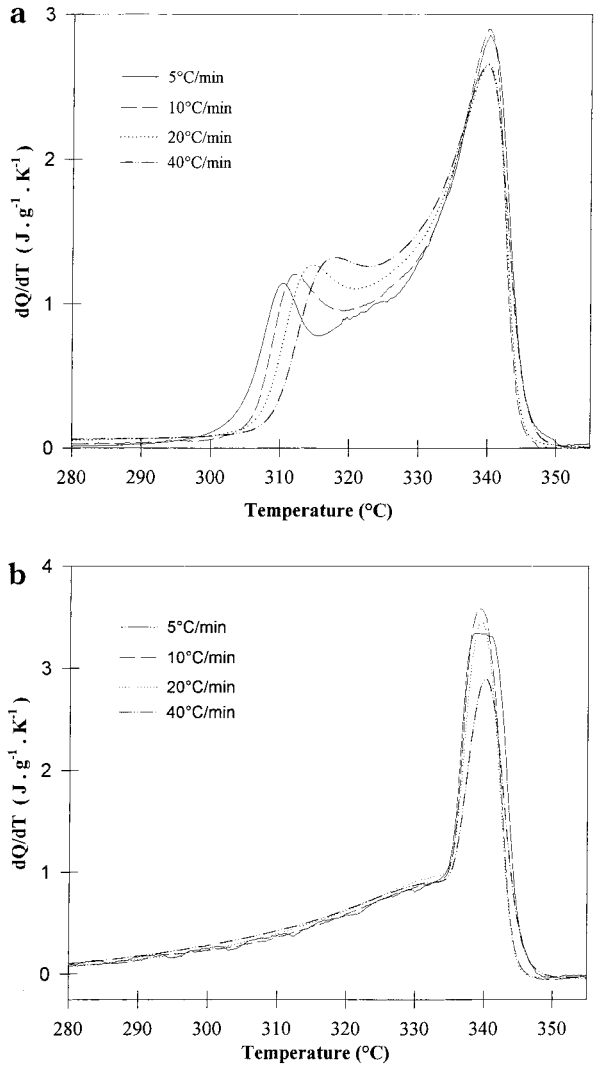

Figure 1. Heating traces at various heating rates after correction with Gray's method[29,30] (a) for MC-300 (t_x = 1000 min) and (b) for MC-300 (t_x = 1000 min) after partial melting at 334 °C.

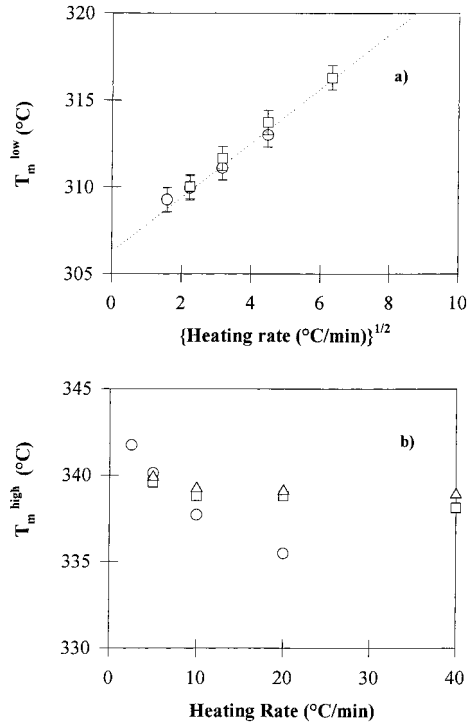

Figure 2. Dependence of (a) the low and (b) the high endotherm peak temperatures on heating rate for MC-300 (□), MC-300 after partial melting at 334 °C (△), and GA-300 (○). Use of the square root of heating rate for T_m^{low} is discussed in ref 34 for bisphenol A polycarbonate.

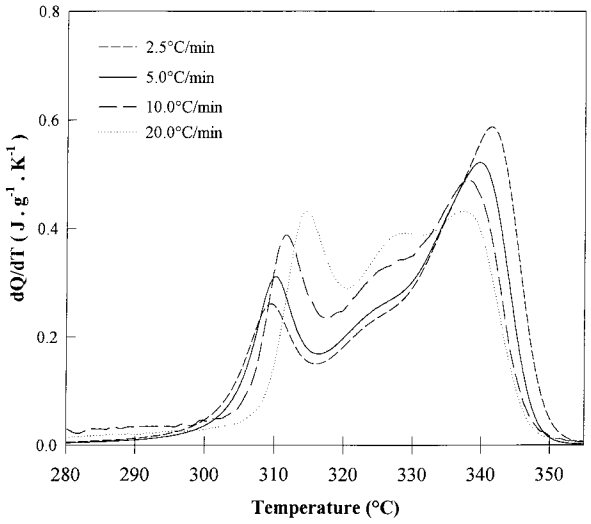

Figure 3. Heating traces at various heating rates after correction with Gray's method[29,30] for GA-300 (t_x = 1000 min).

evolution of the multiple melting behavior with crystallization time. We focus first on samples crystallized from the melt at 290, 300, 310, and 320 °C (samples MC-T_x). In Figure 4, we show typical melting traces after crystallization at T_x = 300 °C for times ranging from 10 to 900 min. The high endotherm melting temperature, T_m^{high}, is independent of crystallization time, and the associated enthalpy of fusion very rapidly reaches its maximum value (in less than 2 min for crystallization at 300 °C). The low endotherm develops noticeably only after primary crystallization and shifts to higher temperature for longer crystallization times. In Figure 5, we show the variation of the low endotherm peak melting temperature, T_m^{low}, with crystallization time on a logarithmic scale for the four melt−crystallization temperatures investigated. The crystallization times used in Figure 5 were corrected by subtracting the induction period for crystallization, correction of significance only for T_x = 320 °C. In all cases, T_m^{low} increases linearly with the logarithm of crystallization time according to the empirical equation

$$T_m^{low}(T_x, t_x) = T_x + A(T_x) + B(T_x)\log(t_x) \qquad (1)$$

where $A(T_x)$ and $B(T_x)$ are given in Table 1. It is interesting to note that extrapolation of T_m^{low} to very short crystallization times (ca. few seconds) yields within a fraction of a degree the crystallization temperature.

We now focus on the effect of primary crystallization conditions on the temporal evolution of the low endotherm position after secondary crystallization at 300 °C. We compare the behavior of melt crystallized samples MC-300 and MC-300-PM-SC-300 with that of cold crystallized samples GA-300 and GA-300-PM-SC-300. In Figure 6, we show that the evolution of the low endotherm melting temperature with time is very similar for samples undergoing secondary crystallization at 300 °C, whether primary crystallization takes place

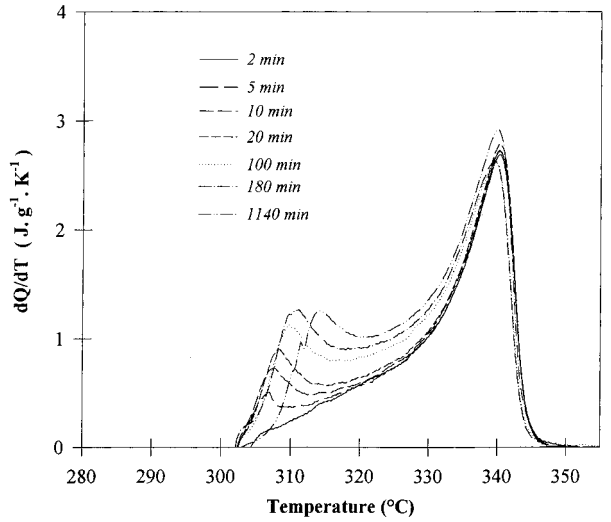

Figure 4. Heating traces (HR = 10 °C/min) of MC-300 crystallized for times ranging from 10 to 900 min.

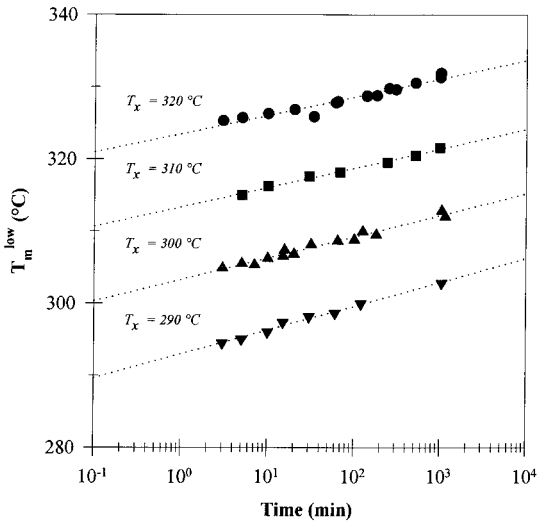

Figure 5. Evolution of the low endotherm peak temperature with crystallization time for MC-290, MC-300, MC-310, and MC-320 (HR = 10 °C/min).

Table 1. Parameters Describing the Temporal Evolution of the Low Endotherm for Different Thermal Histories

sample series	$A(T_x)$	$B(T_x)$	n	T_{pm}	$C(T_x)$	$D(T_x)$
MC-290	4.1	3.0	0.50	NA	3.1	1.3
MC-300	4.1	2.6	0.50	NA	3.8	1.4
MC-310	3.7	2.6	0.60	NA	2.8	1.9
MC-320	3.2	2.3	*a*	NA	*a*	*a*
MC-300-PM-SC-300	4.8	2.5	0.49	334	2.7	1.8
MC-300-PM-SC-320	5.6	2.3	0.87	334	7.6	0.7
MC-300-PM-SC-210	6.5	4.7	0.24[c]	334	*b*	*b*
MC-300-SC-210	6.8	4.6	*b*	NA	*b*	*b*
GA-210	5.9	4.9	*b*	NA	*b*	*b*
GA-300	5.3	2.7	0.47	NA	2.8	1.7
GA-300-PM-SC-300	5.4	2.5	0.56	334	2.3	1.9
GA-300-PM-SC-320	5.7	1.8	0.86	334	1.8	2.7
GA-300-PM-SC-210	6.1	4.9	0.23[c]	334	*b*	*b*

[a] Was not calculated due to overlap between primary and secondary crystallization. [b] Was not calculated because of melting recrystallization effects above the low endotherm. [c] Without physical significance (see text).

from the melt or from the glass and whether samples were partially melted at 334 °C. Only small variations in the parameters $A(T_x)$ and $B(T_x)$ with primary crystallization history are observed (Table 1).

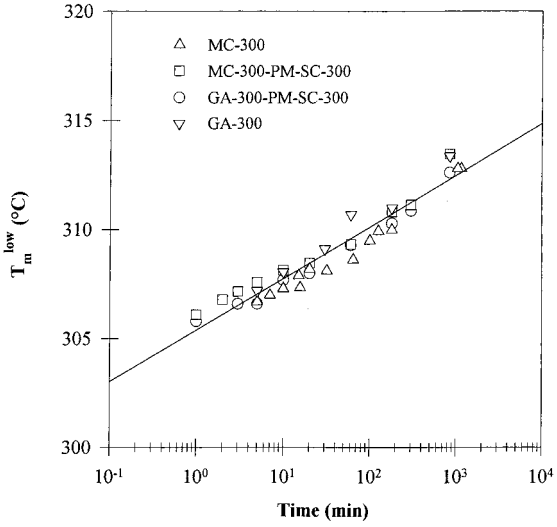

Figure 6. Evolution of the low endotherm peak temperature with time for secondary crystallization at 300 °C, after different primary crystallization histories.

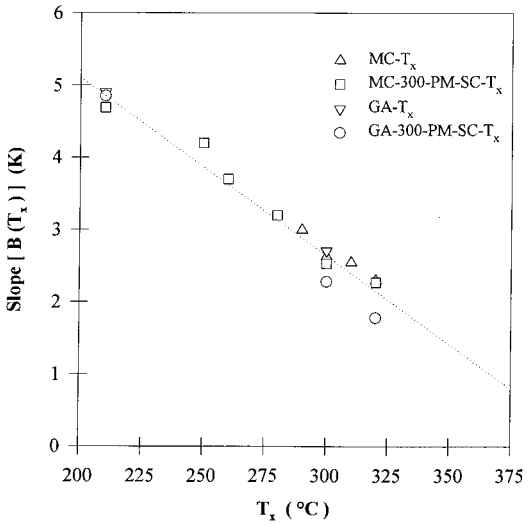

Figure 7. Temperature dependence of the rate of upward shift, $B(T_x)$, of the low endotherm after secondary crystallization at T_x. $B(T_x)$ is calculated from DSC heating traces recorded at 10 °C/min for crystallization times given in minutes.

The influence of primary crystallization conditions on the evolution of the low endotherm position was also studied for secondary crystallization at 210 °C. Examination of Table 1 for samples GA-210, GA-300-PM-SC-210, and MC-300-SC-210 indicates that $B(T_x)$, the rate of upward shift of the low endotherm position with secondary crystallization time, is barely dependent on primary crystallization conditions.

Secondary crystallization experiments were also carried out under a variety of conditions for temperatures ranging from 180 to 320 °C (see Table 1). The plot of $B(T_x)$ vs secondary crystallization temperature, shown in Figure 7, demonstrates an unambiguous linear correlation between these two quantities. The lower the secondary crystallization temperature, the larger the rate at which the low endotherm shifts to higher temperatures. We note slight but statistically meaningful differences in the magnitude of $B(T_x)$ with primary crystallization conditions only for secondary crystallization at the highest temperatures.

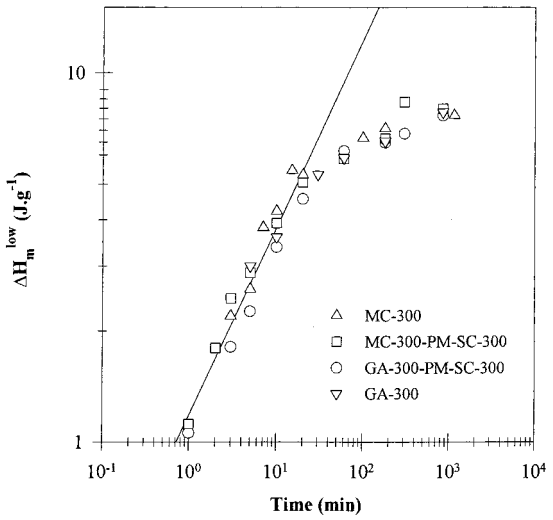

Figure 8. Avrami plot for secondary crystallization at 300 °C in the context of the free growth approximation for samples with different primary crystallization histories.

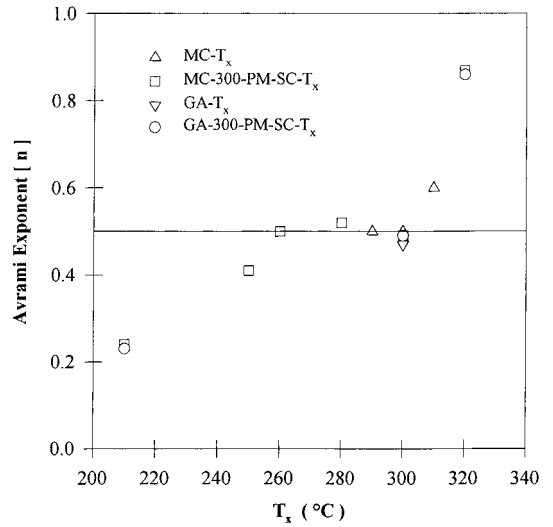

Figure 9. Evolution of the Avrami exponent with secondary crystallization temperature.

Low Endotherm Enthalpy of Fusion (Short Annealing Times). We now address the crystallization time dependence of the enthalpy of fusion associated with the low endotherm. For each crystallization condition, the corresponding heating trace was analyzed using the peak deconvolution method previously discussed for ethylene/α-olefin copolymers.[1,2] We note that the evolution of the low endotherm enthalpy of fusion with secondary crystallization time is similar for samples crystallized from the melt, from the glassy state, and for samples partially melted after primary crystallization. In Figure 8, in the context of the free growth approximation,[31] $\log(\Delta H_f^{low})$ is plotted versus $\log(t_x)$ for samples undergoing secondary crystallization at 300 °C after various primary crystallizations. The slope of such a plot at the early stage of secondary crystallization defines the Avrami exponent, *n*. In all cases, an Avrami exponent in the vicinity of $^1/_2$ is obtained (Table 1). This analysis was repeated for PEEK samples undergoing secondary crystallization at different temperatures, and the corresponding Avrami exponents are shown in Table 1 and plotted in Figure 9. When the secondary crystallization process is monitored at temperatures identical to or lower than the primary crystallization temperature, *n* is generally in the vicinity of $^1/_2$. We note, however, that an increase in Avrami exponent with crystallization temperature is observed for crystallization above 300 °C. We also note that for relatively low secondary crystallization temperatures (210 and 240 °C) the Avrami exponent apparently decreases below $^1/_2$, an issue which is addressed further in the next section.

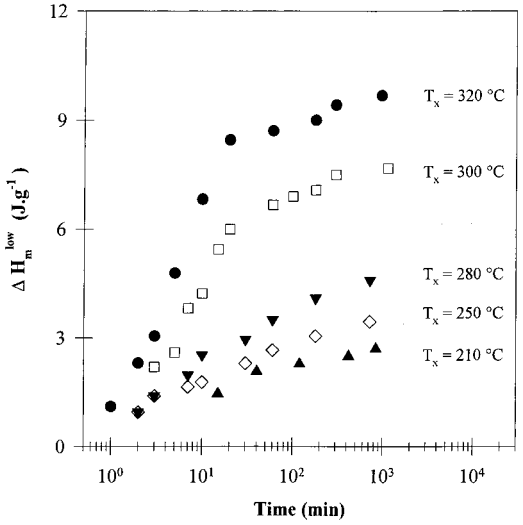

Figure 10. Evolution of the low endotherm enthalpy of fusion with time (full lines indicate the long time limiting behavior, i.e., the second stage of secondary crystallization).

Low Endotherm Enthalpy of Fusion (Long Annealing Times). Examination of Figure 8 suggests that secondary crystallization at 300 °C occurs in two stages. Whereas the initial stage can be described with an Avrami exponent of $^1/_2$, a departure from this behavior is observed at longer times. If the enthalpy of fusion associated with the low endotherm is plotted as a function of the logarithm of time, a linear behavior is observed in the long time limit (Figure 10). Thus, ignoring the early stages of secondary crystallization, the heat of fusion is well represented by the empirical equation

$$\Delta H_f^{low} = C(T_x) + D(T_x)\log(t_x) \qquad (2)$$

where $D(T_x)$ is plotted as a function of temperature in Figure 11. The clear delineation of two stages of secondary crystallization is observed at all but the lowest crystallization temperatures (i.e., only for $T_x \geq 260$ °C). Examination of the evolution of the low endotherm enthalpy of fusion with time for secondary crystallization temperatures below 260 °C indicates that ΔH_f^{low} varies linearly with $\log(t_x)$ over the whole range of crystallization times. This suggests that, first, at low temperatures the initial secondary crystallization stage (with $n = {}^1/_2$) is not detected, and second, Avrami exponents lower than $^1/_2$ estimated for $T_x < 260$ °C and plotted in Figure 9 have no physical meaning. Indeed, examination of Figures 10 confirms that only the second stage of secondary crystallization is observed for $T_x < 260$ °C. Observation that the maximum degree of crystallinity developed during secondary crystallization decreases with decreasing temperature (Figure 10) suggests that a limitation in instrumental sensitivity prevents the observation of the initial stage of secondary crystallization below 260 °C.

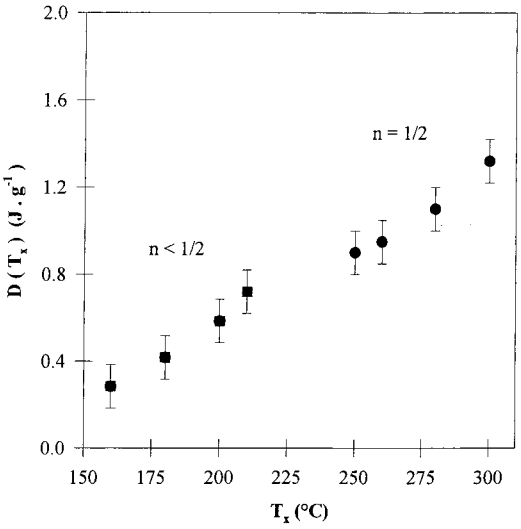

Figure 11. Evolution of the rate of secondary crystallization (quantity $D(T_x)$ in eq 2) with temperature in the long time limit.

3. Two-Step Crystallization Studies. In this section, we report the results of two-step crystallization experiments. These experiments are designed to investigate, first, the origin of the upward shift of the low endotherm to higher temperatures with longer crystallization times and, second, to gain further insight into the nature of the crystals melting at low temperatures.

In the first series of experiments, PEEK was crystallized at 300 °C for 60 min and subsequently quenched to 210 °C where further crystallization was allowed for different times ranging from 10 to 1000 min. DSC heating traces for this series of samples are shown in Figure 12a. Four endotherms are observed in all cases. The upper two endotherms are associated with the melting of primary and secondary crystals formed at 300 °C and exhibit enthalpies of fusion and peak melting temperatures identical to those described above for sample MC-300. The shallow endotherm centered around 270 °C is likely to be associated with the melting of crystals formed during cooling from 300 to 210 °C. The lowest endotherm, on the other hand, is associated with the melting of crystals formed at 210 °C. The crystallization time dependencies of the lowest endotherm enthalpy of fusion and peak melting temperature are identical to those determined above for samples undergoing secondary crystallization at 210 °C. The location of the next-to-highest endotherm is independent of residence time at 210 °C, although the crystals which melt at this endotherm were stored at 210 °C for different times. Similar experiments were carried out for smaller temperature intervals between T_{x1} and T_{x2} (i.e., T_{x2} = 240 or 280 °C). In these cases, the location of the next-to-highest endothermic transition was also observed to be independent of residence time at the lowest crystallization temperature.

In the second set of experiments, PEEK was melt-crystallized at 300 °C for times ranging from 10 to 1000 min and subsequently quenched to 210 °C, where it was allowed to crystallize further for a fixed time (110 min). DSC heating traces are shown in Figure 12b. Four endotherms are also observed in all cases. The upper two endotherms are identical to those discussed earlier for the MC-300 sample. The lowest endotherm is identical to that expected for a sample undergoing secondary crystallization at 210 °C. In the present case, the lowest

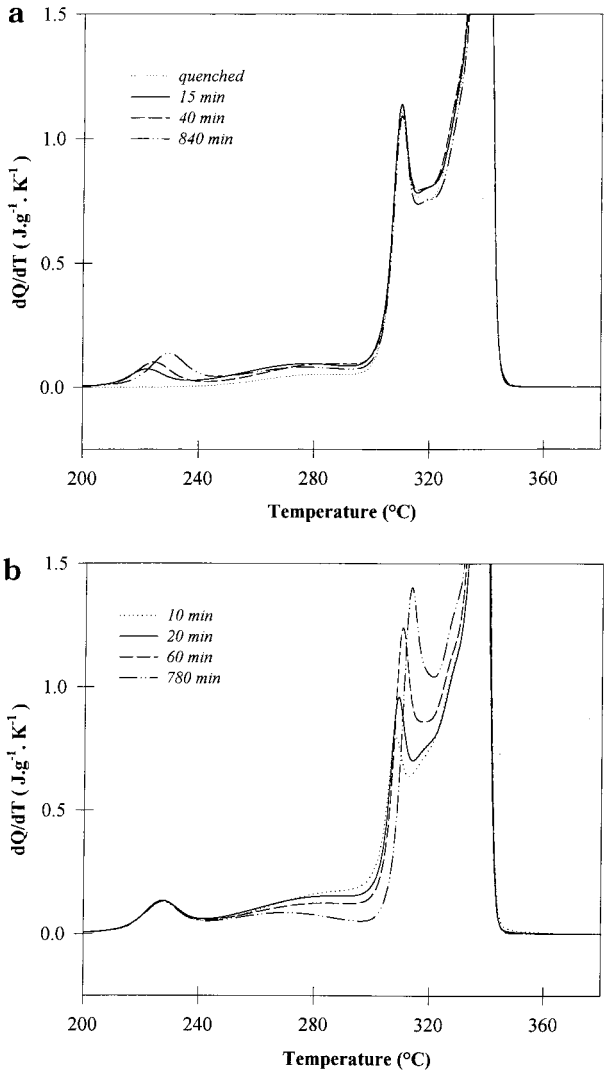

Figure 12. Heating traces after two-step crystallization experiments: (a) T_{x1} = 300 °C, t_{x1} = 60 min, T_{x2} = 210 °C, t_{x2} variable; (b) T_{x1} = 300 °C, t_{x1} = variable, T_{x2} = 210 °C, t_{x2} = 110 min.

and highest endotherms show no dependence on residence time at 300 °C. The crystallization time dependence of the next-to-highest endotherm location matches exactly that discussed for sample MC-300. As expected, when the crystallization time is increased at 300 °C, the low endotherm associated with secondary crystallization at 300 °C (i.e., the next-to-highest endotherm) increases in magnitude. However, under these conditions we observe a concomitant decrease in the apparent heat capacity just below that endotherm. Thus, an increase in residence time at 300 °C leads to a larger population of crystals that melt just above 300 °C and a smaller population of crystals that form during cooling at temperatures slightly below 300 °C. Indeed, the apparent heat capacity between 300 and 260 °C decreases steadily as the crystallization time at 300 °C is increased. We recall that the population of crystals formed at 210 °C is not affected by the residence time at 300 °C. This suggests that a fraction of the amorphous phase remaining after crystallization at 300 °C is able to crystallize at 210 °C but cannot do so at 300 °C for the chosen residence times at that temperature.

4. Glass Transition Behavior. The variation in glass transition temperature with crystallization time

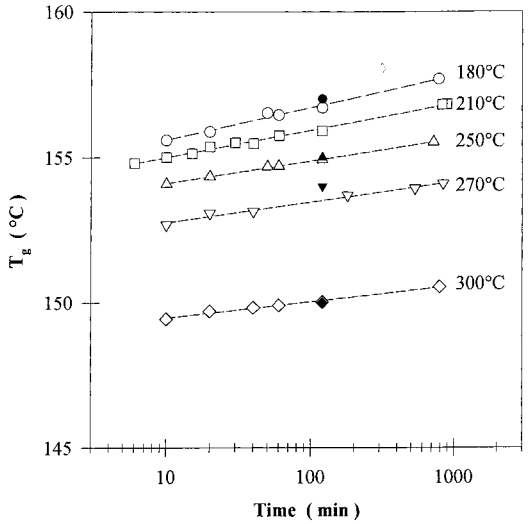

Figure 13. Evolution of the glass transition temperature with secondary crystallization time for samples GA-180, GA-210, GA-250, GA-270, and GA-300 (open symbols this work, full symbols from Cheng et al.[14]).

was investigated for samples annealed at a temperature T_a for different times (samples GA-T_a where T_a = 180, 210, 250, 270, and 300 °C). Care was taken to use precisely the same cooling rate and residence time below T_g after all crystallization experiments to avoid artifacts due to different extents of aging below T_g. Within the experimental uncertainty, the glass transition temperature increases linearly with the logarithm of secondary crystallization time (Figure 13) according to

$$T_g(T_a,t_a) = a(T_a) + b(T_a)\log(t_a) \qquad (3)$$

The quantity $b(T_a)$, the rate of upward shift of T_g with $\log(t_a)$, increases with decreasing annealing temperature. Data in Figure 13 also confirm earlier reports that, for a fixed crystallization time, the glass transition temperature increases with decreasing cold-crystallization or annealing temperature.[14]

Discussion

1. Heating Rate Studies. Many studies of the heating rate dependence of the multiple behavior of PEEK have been reported in the literature.[6−8,11,14,16,20,21] In some studies, the observed shifts of the low and high endotherms with heating rate were used to explain the multiple melting behavior by a melting−recrystallization−remelting process.[6−8,11] In other studies, the same experiments were used to conclude that the low and high endotherms are associated with the melting behavior of separate populations of crystals.[16,20,21] Careful inspection of these studies provides a number of hints as to the origin of this confusion. First, heating rate studies of cold-crystallized PEEK suggest significant melting−recrystallization−remelting during heating, while those on melt-crystallized PEEK indicate, at most, very minor reorganization. Second, in previous studies, the correction of melting traces for thermal lag effects was simply accomplished through shifts in the temperature scale using the melting scan of an indium standard at the appropriate heating rate. It is known that an increase in heating rate leads not only to an artificial shift of the melting transition to higher temperatures but also to a broadening of the endotherms.[1,30] When a heating trace displays multiple melting transitions in a narrow temperature range, it is important to account for the effect of heating rate on the shape of the endotherm. This can be accomplished as a first approximation using the method developed by Gray.[29,30]

Our studies (Figure 2) show that the location of the high endotherm of melt-crystallized PEEK is independent of heating rate and of whether the samples were partially melted. A general conclusion drawn from the melt-crystallized samples is that the expected upward shift in temperature and increase in enthalpy of fusion for the high endotherm with decreasing heating rate[32] are not observed, except possibly at the lowest heating rate (5 °C/min). Therefore, if melting−recrystallization−remelting effects are present at all, they are very weak. On the other hand, significant reorganization effects are apparent in the case of PEEK samples crystallized by heating from the glassy state. First, a dramatic decrease in both the high endotherm peak temperature and enthalpy of fusion are observed when the heating rate is increased from 2.5 to 20 °C/min (Figures 2 and 3). Concomitantly, the development of an intermediate endotherm at ca. 330 °C is observed.

We also noted earlier that the upward shift of the low endotherm with increased heating rate is identical for melt and cold-crystallized samples. Should melting−recrystallization−remelting be at the origin of the multiple melting behavior, we would expect significantly different temporal evolutions for the low endotherm in sample MC-300, MC-300-PM-SC-300, GA-300-PM-SC-300, and GA-300. Results reported in Figures 6 and 8 clearly indicate otherwise. Therefore, we conclude that for samples crystallized from the glass or from the melt the multiple melting behavior is indicative of a bimodal population of crystals present at the beginning of the heating scans. In the case of both melt and cold-crystallized PEEK, the low endotherm is associated with the melting of crystals of lower stability, while the high endothermic region is associated with the melting of the most stable crystals. As mentioned above for melt-crystallized samples, the vast majority of the most stable crystals are present at the beginning of the heating scan, and only a small fraction may form through the process of melting−recrystallization−remelting if the heating rate is lower than ca. 5 °C/min. On the other hand, for cold-crystallized samples, the most stable crystals melt predominantly at the intermediate endotherm. The highest endotherm is, in turn, associated with the final melting of material that has undergone a process of melting−recrystallization−remelting during the heating scan. Furthermore, the existence or absence of reorganization during heating in this high molar mass commercial PEEK sample is related to whether crystallization takes place from the melt or the glass but does not correlate with the existence or nature of the low endotherm. While this conclusion should hold for PEEK samples of rather high molar masses, one should be aware that the rate of reorganization during heating increases with decreasing chain length. In fact, a lower molar mass PEEK sample (grade 150G), crystallized from the melt under similar conditions as reported here, does show extensive reorganization during heating.[33] Similar observations were made in our laboratory for bisphenol A polycarbonate.[34]

The rise in the low endotherm melting temperature with heating rate, observed after correction of thermal lag effects, is explained by superheating effects, as discussed by Wunderlich[35] and Zachmann.[36] Anticipat-

ing conclusions drawn later in this paper but introduced earlier for random ethylene/α-olefin copolymers,[1,2] we associate the low endotherm with the melting of secondary crystals in a conformationally constrained environment. We suggest that, in the case of PEEK, this melting process results in the formation of a nonequilibrium amorphous fraction, which is characterized by a lower molar entropy than that of the metastable unconstrained melt at the same temperature. The heating rate dependence of the low endotherm location, after correction using Gray's method, is insignificant for ethylene copolymers[1] but not for PEEK. This variance in behavior may be explained by large differences in the relaxation time associated with segmental reorientation during the melting of secondary crystals. We assume that melting is a two-step process involving the loss of crystallographic registration and the subsequent randomization of orientation of formerly crystalline segments. An increase in heating rate would lead to a decrease in the apparent entropy of fusion and, thus, to an increase in the observed melting temperature (i.e., to superheating) since less time is given for the randomization step. Finally, we note that the superheating effects discussed here for PEEK have also been observed for secondary crystals melting at the low endotherm in the case of bisphenol A polycarbonate,[34] PET, and it-PS.[37]

2. Secondary Crystallization Process. We define primary crystallization as the stage that ends at spherulitic impingement (i.e., when lamellar growth is no longer taking place from the melt). Since the morphology resulting from primary crystallization is kinetically controlled, it is not surprising to observe that the degree of crystallinity at the end of this stage is significantly below unity. We then define the term secondary crystallization as including any process that leads to further increase in crystallinity and that is not associated with a chain folding lamellar growth mechanism from the free melt.

We envision two main secondary crystallization mechanisms. First, for polymers that exhibit a crystal α_c-relaxation,[38] there will be sufficient mobility in the crystal phase at temperatures between $T\alpha_c$ and T_m to allow isothermal lamellar thickening. This solid-state thickening mechanism is driven by the reduction of the specific surface of lamellar crystals. Except for a few flexible chain polymers with small repeat units, such as linear polyethylene, poly(ethylene oxide), poly(oxymethylene), poly(vinylidene fluoride), and isotactic poly(propylene) which exhibit α_c relaxations, the vast majority of crystallizable polymers are constituted by large and bulky repeat units, which apparently do not exhibit significant translational motion within their crystal phase.[38] For such polymers and for flexible polymers below their α_c relaxation, isothermal lamellar thickening is therefore not a viable option for an increase in crystallinity. For this latter class of polymers, secondary crystallization involves the formation of new crystals with the spherulitic structure formed during primary crystallization.

Previous studies have shown that PEEK's primary crystallization is associated with the formation of spherulites composed of lamellae radiating from a central nucleus.[16,39,40] These results are consistent with reports of an Avrami exponent in the vicinity of 3 for the primary crystallization of PEEK.[15] Comparison of calorimetric and morphological investigations of the melt crystallization of PEEK at 300 °C (Figure 4) indicates that the high endotherm enthalpy of fusion levels off at crystallization times commensurate with spherulitic impingement.[17] Hence, we can unambiguously associate the high endotherm with the melting of primary lamellae forming the spherulitic superstructure.

X-ray scattering,[27,41−44] TEM,[16,40] and low strain momentary creep[25] studies of PEEK indicate that the morphology and mechanical properties continue to evolve well beyond the impingement time, implying the existence of a secondary crystallization stage. For this material, the melting temperature associated with the high endotherm is independent of crystallization time (Figure 4 and refs 14, 16, and 27), indicating that lamellar thickening does not take place in the temperature range investigated. This, in turn, means either that PEEK does not exhibit a crystal α_c relaxation or that this relaxation is located at higher temperatures. Thus, in PEEK, secondary crystallization involves the formation of new crystals. Examination of Figure 4 suggests that the melting of secondary crystals occurs at the low endothermic transition. Support for this statement is provided by the similar time scales associated with the evolution of the low endotherm, the morphology, and the mechanical properties.[25,27] It is important to emphasize that the terminology used here for primary and secondary crystals differs markedly from the concept of dominant vs subsidiary lamellae introduced by Bassett. While we do not anticipate the dominant and subsidiary lamellae to have in general significantly different thermal stabilities, we consider here that primary and secondary crystals form by different mechanisms and exhibit large differences in melting behavior (see below).

Studies of the temporal evolution of the low endotherm enthalpy of fusion show that the rate of secondary crystallization decreases with time (Figure 8). However, this is not an indication that the samples are reaching their ultimate crystallinity, since two-step crystallization experiments show that further crystallization can readily take place upon cooling to lower temperatures (Figure 12a,b). Indeed, Cheng et al.[14] showed that additional crystallinity develops during cooling after isothermal crystallization, even when crystallization times are much longer than the impingement time. Similarly, Chang[13] previously demonstrated that well-defined endotherms develop when PEEK is crystallized at successively lower temperatures. Each crystallization step results in the development of an endotherm located just above the crystallization temperature. In summary, secondary crystallization will occur at or below the primary crystallization temperature to an extent that decreases with decreasing temperature. One might be tempted to explain this behavior by a mechanism of fractionation during primary crystallization.[18,36] However, we refute this explanation since a similar multiple melting behavior is observed in narrow fractions of poly(arylene ether ether ketone),[26] isotactic polystyrene,[45] and bisphenol A polycarbonate.[3]

We now turn our attention to crystallization studies carried out below ca. 310 °C. Annealing from the glassy state (between 180 and 300 °C) or crystallization from the melt (between 280 and 310 °C) leads to very fast primary crystallization (less than ca. 2 min), thus allowing the investigation of the much slower secondary crystallization process independently from primary

crystallization. Partial melting experiments presented in the previous section provide us with samples in which isothermally formed secondary crystals were removed. In bisphenol A polycarbonate,[3,34] cooling after isothermal crystallization and partial melting preserves, to a great extent, the morphology associated with primary crystallization. This can be readily explained by the absence of crystallization during cooling after partial melting. In the case of PEEK, however, this is not the case as this polymer crystallizes very rapidly during cooling below 300 °C. Indeed, the heating trace of a sample crystallized at 300 °C for 1000 min, partially melted at 334 °C, and quenched to room temperature exhibits a low-temperature tail extending to below 280 °C (Figure 1b), indicating further crystallization during cooling. Despite this shortcoming, important information can be extracted from secondary crystallization experiments in partially melted PEEK. The results are discussed below in more detail.

An Avrami exponent of $^1/_2$ characterizes secondary crystallization at temperatures below 310 °C. The melting point of secondary crystals increases linearly with the logarithm of crystallization time. We showed in Figure 5 that the melting temperature of these crystals could be extrapolated at short times to a value in the vicinity of the crystallization temperature, from which we conclude that these crystals are, at least initially, of small lateral dimensions. From these and similar observations for ethylene/1-octene copolymers,[1] we furthermore conclude that the morphologies associated with crystals melting at the high and low endotherms are necessarily different. Morphological studies of PEEK, in our opinion, have not provided definitive information as to the nature of secondary crystals or their location within the spherulites.[16,18] The striking similarities between secondary crystallization of ethylene/α-olefin copolymers,[1,2] isotactic polystyrene,[26,34,46] and PEEK lead us to speculate that the morphology of crystals associated with the low endotherm should be similar for these materials. In the case of ethylene/α-olefin copolymers, we inferred from atomic force microscopy observations that secondary crystallization leads to the formation of bundled chain (fringe-micellar) crystals of limited lateral dimensions.[1,2] A similar morphology may also apply for PEEK, when secondary crystallization is carried out at temperatures below 310 °C. The rationale for this speculation is based on the fact that crystallization of semiflexible chain polymers, such as PEEK, cannot involve frequent adjacent reentry folding because of local chain rigidity.[47] In support of this argument, we recall that the lamellar structure of PEEK is comprised of thin mosaic-block structures of small lateral dimensions.[39,40,48] We also recall reports on the difficulty to grow large facetted single crystals of PEEK from dilute solution.[39,48] Poor facetting and small lateral crystal dimensions usually arise from a lack of regularity in the chain folding process and, thus, from steric stresses at the crystal basal planes. PEEK primary crystals may bear more resemblance to the switchboard model of Flory than to the regularly and tightly chain folded model of Keller. Partial crystallization of polymer chains during the primary stage lead us to anticipate the existence of a distribution of folds, cilia, and tie chains of various lengths. We can now propose an explanation for the similarity in secondary crystallization behavior between semiflexible homopolymers such as PEEK and flexible random ethylene/1-octene copolymers. In the latter case, crystallizable sequences are defined as the methylene sequences between hexyl branches. In the case of PEEK, they are the chain sections in interlamellar amorphous layers, pinned at one or both ends on previously formed crystals. The concept of a distribution of loose fold, cilium, or tie chain lengths is analogous to that of a distribution of crystallizable sequence lengths in a copolymer of crystallizable A units and noncrystallizable B units. Thus, the length, local concentration, and segmental mobility of these folds, cilia, and tie chains dictate the temperature and the rate at which some of their segments will crystallize during cooling (Figure 12a,b). As a sample is brought to lower temperatures, progressively shorter and more constrained sections of chains are expected to take part in the secondary crystallization process, giving rise to crystals of steadily decreasing thermal stability. Secondary crystallization at the highest temperatures must involve the longest loose folds, cilia, and tie chains. In contrast, secondary crystallization at the lowest temperatures may be described as a clustering of a few repeat units belonging to the same or neighboring chains. In the case of PEEK, the final morphology is primarily controlled by the crystallization times and temperatures associated with the primary and secondary stages but also affected by each of the cooling steps between isothermal treatments.

The results presented in Table 1 indicate that the kinetic parameters describing secondary crystallization at T_x are within experimental error identical for samples either annealed from the glass by heating to T_x or crystallized from the melt at T_x with or without partial melting. A slightly lower value of $B(T_x)$ is observed for samples undergoing secondary crystallization after annealing from the glass and partial melting. This latter observation only holds for secondary crystallization temperatures equal to or above the primary crystallization temperature (i.e., for $T_x = 300$ or 320 °C but not for $T_x = 210$ °C) and provides further support for the idea that reorganization during heating occurs only for cold-crystallized samples. It also suggests that the cooling stage between primary and secondary crystallization temperatures and the resulting increase in crystallinity and constraints play a considerable role in controlling the kinetic parameters associated with secondary crystallization at lower temperatures (e.g., 210 °C in the present case). The observation that the secondary crystallization kinetics at low temperatures does not depend on whether partial melting is carried out or not is consistent with the notion introduced earlier for ethylene copolymers[1] and poly(ethylene terephthalate)[49] that the degree of crystallinity changes reversibly during cooling and subsequent heating below the primary crystallization temperature. This latter assertion also follows from the observation that the low endotherm extrapolates to the secondary crystallization temperature at short times (i.e., "young" secondary crystals appear to melt reversibly; see Figure 5 and values for A and B in Table 1). Indeed, following arguments proposed by Flory[50] which are compatible with Gambler's ruin concepts,[51] secondary crystals must be of limited lateral dimensions in the absence of significant chain folding. In contrast, we note that the initial melting point of secondary crystals formed at the highest temperatures departs more significantly from the crystallization temperature (see samples MC-320, MC-300PM-SC-320, and GA-300-PM-SC-320 in Table

1). Formation of the largest crystals from the longest sequences can be understood in terms of secondary crystallization under conditions of least constraints.

Let us now discuss secondary crystallization at temperatures above ca. 310 °C. As the crystallization temperature is raised, differences in thermal stability between primary and secondary crystals diminish, suggesting that primary and secondary crystals become morphologically similar only at the highest crystallization temperatures. A systematic evolution of the secondary crystal morphology above ca. 310 °C may also be inferred from the departure of the Avrami exponent from the value of $^1/_2$ (characterizing fringe-micellar-like secondary crystals) and its steady increase above that temperature.

Previous DSC studies indicate that the degree of primary crystallinity reached under isothermal conditions decreases with crystallization temperature above 300 °C.[14−17] It is well-known that spherulite coarseness increases with temperature.[17,40] Under such conditions a greater regularity in lamellar stacking but also larger interfibrillar or interstack regions are observed. The classical work of Keith and Padden[52] suggests that this behavior results from the rejection of impurities (fractionation) away from the multiple growth fronts of a lamellar stack. Although such a mechanism is certainly operative in impure melts, we believe it is not sufficient to explain our results in semiflexible polymers since similar coarsening and multiple melting behavior are also observed in narrow molecular weight fractions of PEEK,[26] highly isotactic polystyrene,[45] and bisphenol A polycarbonate.[3] We would like to argue that the increase in coarseness and the appearance of interfibrillar amorphous regions is associated with a decrease in the frequency of screw dislocations at higher crystallization temperatures. Indeed, noncrystallographic lamellar branching is often associated with the existence of screw dislocations.[53] As the crystallization temperature is increased, crystal growth proceeds in a more equilibrium-like fashion leading to thicker and larger lamellae, thus suggesting a lower magnitude for the interfacial stresses due to steric repulsions between amorphous sequences escaping the crystal surface. The resulting decrease in the frequency of screw dislocations would certainly lead to an increase in the regularity of lamellar stacking but would also result in more significant interfibrillar regions, since a decrease in branching frequency prevents growing crystals from exploring more of the uncrystallized free melt. Therefore, more significant interfibrillar regions are formed at higher crystallization temperatures, leading to a higher extent of secondary crystallization. Support in favor of this argument stems from the observation that the ratio of the low to the high endotherm heats of fusion increases with crystallization temperature and appears to be practically independent of molar mass distribution.[17,26]

Secondary crystallization at temperatures above ca. 310 °C would therefore take place in a considerably less constrained environment than at lower temperatures and involve not only long cilia and loose folds but also free chains in the interfibrillar region. Considering the formation of secondary crystals at high temperature, we speculate that these crystals are nucleated from cilia and loose folds at the surface of primary crystals since such sequences are more constrained and thus exhibit a lower conformational entropy and a higher driving force toward crystal nucleation than the free chains located in the interfibrillar region. Similar arguments were proposed by Medellin-Rodriguez et al.[12]

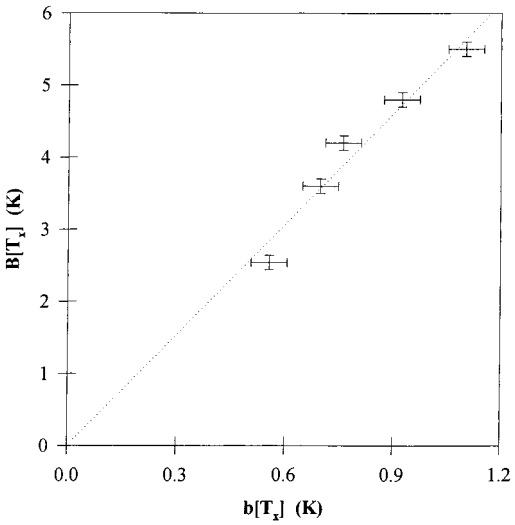

Figure 14. Correlation between $B(T_x)$, the rate of shift of the low endotherm, and $b(T_x)$, the rate of shift of the glass transition, with secondary crystallization time (in minutes).

3. Origin of the Time Dependence of the Low Endotherm Position. Simple thermodynamic considerations indicate that an increase in melting temperature can be associated either with a decrease in the free energy of the crystal phase or with an increase in free energy of the amorphous phase.[1] These two possibilities are now addressed in turn.

Support for an increase in the free energy of the amorphous fraction during secondary crystallization is received from observations that the time and temperature dependences of the low endotherm location are paralleled by those of the glass transition temperature (Figure 13). Indeed, both T_g and T_m^{low} increase linearly with the logarithm of secondary crystallization time, and both $b(T_x)$ and $B(T_x)$ increase with decreasing secondary crystallization temperature. More importantly, a plot of $B(T_x)$ as a function of $b(T_x)$ shows remarkable correlations between these two quantities and appears to extrapolate to the origin (Figure 14). A recent thermodynamic treatment based on conformational entropy arguments indeed shows that the theoretical and experimental values of $B(T_x)/b(T_x)$ compare very well for PEEK, PET, and it-PS if the heating rate dependence of the low endotherm is taken into account.[37] We also note that this specific explanation for the time dependence of the low endotherm location is fully compatible with the interpretation of two-step crystallization studies (Figure 12a) given in a previous publication on ethylene/1-octene copolymers.

Although the above proposal may have some merit, it has recently attracted justifiable skepticism.[54,55] Indeed, a decrease in the free energy of secondary crystals with time can also explain the shift of the low endotherm location to higher temperatures. Three mechanisms leading to a reduction in crystal free energy can be invoked, namely, an increase in crystal thickness, an increase in crystal perfection through better chain packing, and an increase in crystal lateral dimensions. Two-step crystallization studies (see Figure 12a) show that the location of the endotherm located around 310 °C is independent of residence time at 210 °C. Since similar results are also obtained when the two crystallization temperatures, T_{x1} and T_{x2}, differ by less than

20 K, regardless of the temperature range where primary crystallization takes place, we conclude that the shift of the low endotherm with time cannot be explained by an increase in crystal perfection or by a crystal thickening process. Indeed, these two mechanisms are generally explained in terms of defect diffusion processes. We would therefore expect that the rate of increase in crystal perfection or thickness be a smooth and increasing function of temperature. In contrast, $B(T_x)$ decreases with increasing secondary crystallization temperature (Figure 7). So, it appears that if the free energy of secondary crystals does indeed decrease with time, it can only be associated with an increase in their lateral dimensions during secondary crystallization. This explanation may seem a priori incompatible with the observation that the rate of secondary crystallization at long times, $D(T)$ (eq 2 and Figure 11), and the quantity $B(T)$ (Figure 7) have opposite temperature dependences. However, this apparent incompatibility may be lifted if one assumes that secondary crystallization at the higher temperatures yields more rapidly larger crystals which gain little further stability by growing laterally over long periods of time (i.e., small $B(T)$). Conversely, secondary crystallization at lower temperatures would lead to the formation of very small crystals, which could gain significant stability through lateral growth. Indeed, it is well established from Gibbs−Thompson-like treatments that the increase in melting temperature (i.e., stability) with size is most prominent at small sizes. This reasoning also appears to be consistent with the evolution of the initial melting temperature of secondary crystals with crystallization temperature (eq 1, Table 1).

Regardless of the origin of the evolution of the low endotherm with crystallization time, it is clear that the evolution of the glass transition temperature is consistent with a decrease in the conformational entropy of the remaining amorphous fraction as a result of secondary crystallization. Secondary crystallization can then be viewed as a reversible cross-linking process leading to conformational constraints in the remaining noncrystalline fraction. We note that the rate of establishment of these constraints increases with decreasing crystallization temperature. Secondary crystals formed at the lowest temperatures are expected to be smaller and to exhibit fewer chain folds and thus may be more efficient cross-linking sites for the amorphous fraction. Finally, the inference from data presented here and elsewhere that secondary crystallinity varies reversibly with temperature below the primary crystallization temperature[48] and the recognition that secondary crystallization leads to the generation of constraints in the amorphous fraction[56−60] are qualitatively consistent with reports that the rigid amorphous fraction has a negative temperature coefficient.[14,59]

Conclusions

The double melting behavior of PEEK (grade 450G) is explained in terms of a dual population of primary and secondary crystals and does not result from melting−recrystallization−remelting effects during heating. We showed in this paper that the existence or absence of crystal reorganization is associated with whether crystallization takes place from the glass or the melt but does not influence the characteristics of the low endotherm. Reorganization processes primarily affect the shape of the high endotherm.

Secondary crystallization of PEEK is shown to be similar to that previously reported for random ethylene/α-olefin copolymers: after crystallization below a crossover temperature (T^* = ca. 310 °C for PEEK), the melting temperature of secondary crystals is located initially just above the crystallization temperature and increases linearly with the logarithm of time; the initial stage of secondary crystallization is characterized by an Avrami exponent of $^1/_2$ while in the late stage secondary crystallinity increases linearly with the logarithm of time. Above T^*, the Avrami exponent increases with temperature above the value of $^1/_2$, and the initial melting temperature of secondary crystals deviates more significantly from the crystallization temperature. We speculate that secondary crystallization below T^* involves loose folds, tie chains, and long cilia and yields interlamellar fringed micellar structures. As the temperature is raised above T^*, evolution of the melting behavior and Avrami exponent suggests that secondary crystals become more lamellar in nature. In addition, we found that the glass transition temperature of PEEK increases linearly with the logarithm of secondary crystallization time at a rate, $b(T_x)$, which decreases with increasing temperature. The similar temperature dependence of $b(T_x)$ and $B(T_x)$, the rate of upward shift of secondary crystal melting temperature, suggests a common origin for the evolution of the low endotherm and glass transition temperature. We proposed that such a behavior arises from the decrease in conformational entropy of the remaining amorphous fraction as a result of secondary crystallization. We cannot, however, rule out the possibility that a change in the lateral dimensions of secondary crystals with crystallization time is at the origin of the evolution of their melting behavior.

Irrespective of this issue, secondary crystallization can then be viewed as a thermoreversible cross-linking process, whose extent increases with crystallization time and efficiency increases with decreasing crystallization temperature. The qualitative crystallization model proposed here for semiflexible polymers now provides a new venue for understanding the evolution of mechanical properties with time above their glass transition temperature.

Acknowledgment. We acknowledge support of this work by the NSF Science and Technology Center on High Performance Polymeric Adhesives and Composites at Virginia Polytechnic Institute and State University (DMR 91-20004) and by a National Science Foundation Young Investigator Award (DMR 93-57512). We also acknowledge the Perkin-Elmer Corporation for the donation of a differential scanning calorimeter DSC-7.

References and Notes

(1) Alizadeh, A.; Richardson, L.; Xu, J.; Marand, H.; Cheung, W.; Chum, S. *Macromolecules* **1999**, *32*, 6221.
(2) Subramaniam, C. Morphology, Crystallization and Melting Behavior of Random Copolymers of Ethylene with 1-Butene, 1-Pentene and 1-Hexene. Ph.D. Dissertation, Virginia Polytechnic Institute and State University, 1999. Subramaniam, C.; Alizadeh, A.; Marand, H. To be submitted to *Polymer*.
(3) Alizadeh, A.; Sohn, S.; Marand, H.; Iler, H. D.; Schank, L. To be submitted to *Macromolecules*.
(4) Xu, J.; Alizadeh, A.; Marand, H.; Cheung, W.; Guest, M. To be submitted to *Macromolecules*.
(5) Blundell, D. J.; Osborn, B. N. *Polymer* **1983**, *24*, 953.
(6) Blundell, D. J. *Polymer* **1987**, *28*, 2248.
(7) Lee, Y.; Porter, R. S. *Macromolecules* **1987**, *20*, 1336.
(8) Lee, Y.; Porter, R. S. *Macromolecules* **1989**, *22*, 1756.

(9) Jonas, A. M.; Russell, T. P.; Yoon, D. Y. *Macromolecules* **1995**, *28*, 8491.
(10) Fougnies, C.; Damman, P.; Villers, D.; Dosiere, M.; Koch, M. H. J. *Macromolecules* **1997**, *30*, 1385.
(11) Fougnies, C.; Damman, P.; Dosiere, M.; Koch, M. H. J. *Macromolecules* **1997**, *30*, 1392.
(12) Medellin-Rodriguez, F. J.; Phillips, P. J.; Lin, J. S. *Macromolecules* **1996**, *29*, 7491.
(13) Chang, S.-S. *Polymer* **1988**, *29*, 138.
(14) Cheng, S. Z. D.; Cao, M.-Y.; Wunderlich, B. *Macromolecules* **1986**, *19*, 1868.
(15) Cebe, P.; Hong, S. D. *Polymer* **1986**, *27*, 1183.
(16) Bassett, D. C.; Olley, R. H.; Al Raheil, I. A. M. *Polymer* **1988**, *29*, 1745.
(17) Marand, H.; Prasad, A. *Macromolecules* **1992**, *25*, 1731.
(18) Lattimer, M. P.; Hobbs, J. K.; Hill, M. J.; Barham, P. J. *Polymer* **1992**, *33* (18), 3971.
(19) Kruger, K. N.; Zachmann, H. G. *Macromolecules* **1993**, *26*, 5202.
(20) Chen, C.-Y.; Woo, E. M. *Polym. J.* **1995**, *27*, 361.
(21) Ko, T. Y.; Woo, E. M. *Polymer* **1996**, *37*, 1167.
(22) Tan, S.; Su, A.; Luo, J.; Zhou, E. *Polymer* **1999**, *40*, 1223.
(23) Vaughan, A. S.; Stevens, G. C. *Polymer* **1995**, *36*, 1531.
(24) Cebe, P. *J. Mater. Sci.* **1988**, *23*, 3721.
(25) Velikov, V.; Marand, H. *J. Therm. Anal.* **1997**, *49*, 375.
(26) Velikov, V. Time Dependent Properties of Semicrystalline Poly(arylene ether ether ketone) Above and Below the Glass Transition. Ph.D. Dissertation, Virginia Polytechnic Institute and State University, 1996.
(27) Verma, R.; Marand, H.; Hsiao, B. S. *Macromolecules* **1996**, *29*, 7767.
(28) Marand, H.; Alizadeh, A.; Farmer, R.; Elkoun, S. To be submitted to *Macromolecules.*
(29) Gray, A. *Analytical Chemistry*; Plenum Press: New York, 1963; Vol. 1, p 322.
(30) Berstein, V.; Ergov, V. M. In *Differential Scanning Calorimetry of Polymers. Physics, Chemistry, Analysis, Technology*; Ellis Horwood: Chichester, U.K., 1994.
(31) Göler, V. F.; Sachs, G. *Z. Phys.* **1932**, *77*, 281.
(32) Rim, P. B.; Runt, J. P. *Macromolecules* **1984**, *17*, 1520.
(33) Sauer, B. B., private communication.
(34) Sohn, S.; Alizadeh, A.; Marand, H. *Polymer,* in press.
(35) Wunderlich, B. *Macromolecular Physics;* Academic Press: New York, 1976; Vol. 3.
(36) Zachmann, H. G. *Kolloid Z. Z. Polym.* **1969**, *213*, 39.
(37) Marand, H.; Alizadeh, A. To be submitted to *Macromolecules.*
(38) Boyd, R. H. *Polymer* **1985**, *26*, 1123. Boyd, R. H. *Polymer* **1985**, *26*, 1123.
(39) Lovinger, A. J.; Davis, D. D. *J. Appl. Phys.* **1985**, *58*, 2843.
(40) Lovinger, A. J.; Hudson, S. T.; Davis, D. D. *Macromolecules* **1992**, *25*, 1752.
(41) Hsiao, B. S.; Gardner, K.-C. H.; Wu, D. Q.; Chu, B. *Polymer* **1993**, *34*, 3986.
(42) Verma, R. K.; Velivov, V.; Kander, R. G.; Marand, H.; Chu, B.; Hsiao, B. *Polymer* **1996**, *37*, 5357.
(43) Hsiao, B. S.; Sauer, B. S.; Verma, R. K.; Zachmann, H. G.; Seifert, S.; Chu, B.; Harney, P. *Macromolecules* **1995**, *28*, 6931.
(44) Wang, W.; Schultz, J.; Hsiao, B. *J. Macromol. Sci., Phys.* **1998**, *B37*, 667.
(45) Iler, H. D. A Study of the Crystallization Kinetics of Isotactic Polystyrene. Ph.D. Dissertation, Virginia Polytechnic Institute and State University, 1995.
(46) Lemstra, P. J.; Koistra, T.; Challa, G. *J. Polym. Sci., Part A-2* **1972**, *10*, 823.
(47) Waddon, A. J.; Keller, A.; Blundell, D. J. *Polymer* **1992**, *33*, 27.
(48) Lovinger, A. J.; Davis, D. D. *Macromolecules* **1986**, *19*, 1861.
(49) Wunderlich, B. *Bull. Am. Phys. Soc.* **1999**, *44*, 294.
(50) Flory, P. J. *Trans. Faraday Soc.* **1955**, *51*, 848.
(51) Guttman, C. M.; DiMarzio, E.; Hoffman, J. D. *Polymer* **1981**, *22*, 1466.
(52) Keith, H. D.; Padden, F. D., Jr. *Polymer* **1986**, *27*, 1463.
(53) Bassett, D. C. In *Principles of Polymer Morphology*; Alden Press: Oxford, 1981.
(54) Crist, B., private communication; *Macromolecules* **1999**, *32*, 8945.
(55) Grubb, D. T., private communication.
(56) Huo, P.; Cebe, P. *Macromolecules* **1992**, *25*, 902.
(57) Kalika, D. S.; Krishnaswamy, R. K. *Macromolecules* **1993**, *26*, 4252.
(58) Ivanov, D. A.; Jonas, A. M. *J. Polym. Sci., Polym. Phys. Ed.* **1998**, *36*, 919.
(59) Nogales, A.; Ezquerra, T. A.; Batallan, F.; Frick, B.; Lopez-Cabarcos, E.; Balta-Calleja, F. J. *Macromolecules* **1999**, *32*, 2301.
(60) Lu, S. X.; Cebe, P. *Polymer* **1996**, *37*, 4857.

MA9913562